Ionics
https://doi.org/10.1007/s11581-026-07040-x

RESEARCH

Luminol-capped cerium nanoparticle aggregates for fluorescent detection of morpholine in fresh fruits

Sivan Vettarayan[1] · Ramesh Manickam[2] · Simon Deepa[1] · Suseela Jayalakshmi[1]

Received: 24 October 2025 / Revised: 17 January 2026 / Accepted: 19 February 2026

Abstract

Luminol-capped cerium aggregated (Ce-Lum) nanoparticles have been developed as a selective fluorescent sensor for detecting morpholine in fruits and vegetables. Synthesized through a simple one-step ambient process, these nanoparticles combine the unique properties of cerium ions (Ce^{3+}/Ce^{4+}) and luminol. Cerium ions act as efficient electron acceptors, enabling charge transfer interactions, while luminol serves as a strong fluorophore with reactive sites for morpholine binding. Upon aggregation, the hybrid nanostructure enhances energy transfer and surface passivation, suppressing non-radiative recombination and improving quantum yield. This synergistic mechanism results in high signal intensity and ultralow detection limits, even in the presence of interfering species. The sensor exhibits excellent sensitivity, specificity, and selectivity, achieving accurate morpholine detection in complex food matrices. Recovery rates close to 100% and relative standard deviation (RSD) values below 3% confirm its precision and reliability. Demonstrating a linear response with a strong correlation coefficient ($R^2 = 0.981$), the system achieves an exceptionally low detection limit of 0.08 ppb. These results highlight the sensor as a significant advancement in morpholine detection, offering potential for food safety monitoring, environmental tracking, and industrial applications. Its superior performance bridges gaps in real-time contaminant detection, ensuring quality and safety assurance.

Keywords Luminol · Morpholine · Aggregated · Chemiluminescence · Nanoparticles

Introduction

Morpholine, a heterocyclic organic compound with a nitrogen-containing ring structure, has found widespread applications across various industrial sectors due to its versatile properties [1, 2]. From its role as a solvent and corrosion inhibitor to its use in pharmaceuticals and pesticides, morpholine plays a significant role in modern manufacturing processes. However, the presence of morpholine in food raises concerns about its potential health implications and regulatory over sight [3, 4]. This essay explores the multifaceted nature of morpholine, examining its industrial applications, health risks, regulatory framework, and the challenges associated with ensuring food safety in the face of potential adulteration. By delving into these aspects, we gain a comprehensive understanding of morpholine's significance and the imperative need for stringent control measures to safeguard public health and maintain food integrity [5]. While widely used, the use of morpholine in food coatings has been banned in some regions (e.g., the European Union) due to potential health concerns, including the formation of nitrosamines when morpholine reacts with nitrites in food. Nitrosamines are known to be carcinogenic. As a result, many countries now rely on alternative waxes and coatings for food preservation [6].

According to China's national standard GB 2760 − 2014, commonly known as fruit wax, morpholine fatty acid salt is permitted as a film-forming agent for fresh fruits. It is primarily applied after surface treatment and is used in quantities appropriate for production requirements [7]. In the

✉ Simon Deepa
deepajenoroi@gmail.com

✉ Suseela Jayalakshmi
jlakshmi2007@gmail.com

[1] Department of Chemistry, School of Basic Sciences, Vels Institute of Science, Technology and Advanced Studies, Chennai, Tamil Nadu 600117, India

[2] Department of Chemistry, Vel Tech Rangarajan Dr. Sagunthala R&D Institute of Science and Technology, Chennai, Tamil Nadu, India

Published online: 17 March 2026

U.S., it is an EPA-registered pesticide ensuring strict safety compliance. Morpholine is illegal and has no upper limit, according to the European Union Food Additives Database (2019) [8].

The application of high-resolution mass spectrometry using gas chromatography, quadrupole, and orbitrap or Tandem mass spectrometry combined with gas chromatography for morpholine characterization, however, has not been studied or documented. Significant benefits are provided in identifying trace contaminants in intricate food matrices [9, 10]. On the other hand, GC–Orbitrap HRMS offers unparalleled benefits, including high resolution, exceptional mass accuracy, and remarkable sensitivity. This technique accurately screens and quantifies trace compounds in complex food matrices [11, 12]. According to these standards, mass spectrometry analysis must achieve four identification points. Orbitrap HRMS performs full-scan precise mass number detection, with each ion contributing two identification points. This allows for a total of four points (two each for quantitative and qualitative ions), enabling simultaneous quantitative and qualitative confirmation [13]. However, these techniques have limitations, including high costs and time-consuming procedures. Therefore, developing low-cost and rapid methods for detecting morpholine in various food samples is highly important [14].

Conventional analytical techniques such as GC–MS and GC–MS/MS remain widely used for morpholine determination due to their high accuracy and sensitivity; however, these methods require extensive sample preparation, costly instrumentation, and skilled operation, limiting their suitability for routine food safety monitoring [9–12]. Advanced approaches such as GC–Orbitrap HRMS provide trace-level detection with exceptional mass accuracy and reliable qualitative and quantitative confirmation, but their high operational costs and complex data processing further restrict large-scale application [11–13]. Alternative strategies, including chemiluminescence-based assays and fluorescence sensing methods, have gained attention owing to their simplicity, rapid response, and lower cost [15–17]. Nevertheless, chemiluminescence methods often suffer from limited selectivity and matrix interference, while nanomaterial-based fluorescent probes and small-molecule sensors may involve complicated synthesis, limited stability, or suboptimal optical properties [15, 16, 18–22]. Fluorescence assays have gained considerable attention for their rapid detection, cost-effectiveness, and high selectivity [15, 16]. However, problems including complicated fabrication processes and low stability are common with nanomaterial probes and quantum dots. Small molecular probes are widely used for pH detection in biosensors, offering advantages over natural dye-modified probes, which are costly and difficult to modify. These include ease of preparation and cost-effectiveness [18, 19]. More recently, 1-oxa-4-azacyclohexane, commonly known as morpholine, was discovered to significantly catalyse the luminol-H_2O_2 system, generating a strong chemiluminescence (CL) signal. Based on this finding, a novel CL strategy for morpholine quantification was proposed, enabling CL imaging detection. This method offers key advantages, including low cost, simplicity, and rapid response, making it a promising approach for morpholine detection [17]. Benzene ring-based fluorescent probes face limitations like low intensity, short wavelengths, and poor water solubility [20–22].

The present study aims to develop a rapid, sensitive, and cost-effective fluorescent sensing strategy for the selective detection of morpholine in fresh fruits and vegetables. The proposed approach addresses the limitations of conventional chromatographic and high-resolution mass spectrometric techniques, which, although highly accurate, are expensive and time-consuming for routine food safety monitoring. By employing aggregated luminol-capped cerium nanoparticles as a novel fluorescent probe, this work seeks to achieve high selectivity and sensitivity toward morpholine in complex food matrices. Accordingly, this work examines the capability of the proposed fluorescent sensor to provide a reliable, simple, and practical alternative for morpholine detection, contributing to advances in food safety analytical methods.

Materials and methods

Materials

Sigma-Aldrich supplied the luminol (99%) which was used without additional purification. Avra provided the following items, which were utilized exactly as supplied: morpholine, malachite green, vanillin, saccharin, calcium lactate, potassium metabisulfite, calcium chloride dihydrate, starch, and rhodamine B. Pellets of sodium hydroxide and cerium chloride were purchased from Merck and utilized exactly as is (pH = 7.54) buffer throughout the study, (Millipore MilliQsystem, 18.2 πΩcm) Millipore water was utilized as the solvent to produce the solution. In Chennai, Tamil Nadu, India, apples and vegetables were purchased from a neighborhood market.

Synthesis of metal aggregated Luminol

Metal-aggregated luminol nanoparticles were synthesized using a straightforward aqueous method. Briefly, 100 mL of an aqueous $CeCl_4$ solution (0.01% w/w) was stirred at 100 rpm to ensure homogeneous mixing. Subsequently, 2 mL of luminol solution (0.01 mol L^{-1}) was rapidly added to the reaction mixture under continuous stirring. The

reaction was allowed to proceed for 2 h at room temperature (25 ± 2 °C), a condition selected to avoid thermal degradation of luminol and to promote controlled coordination between cerium ions and luminol molecules.

After completion of the reaction, the resulting Ce–Lum nanoparticles were purified by centrifugation at 500 rpm for 5 min to remove excess reactants and loosely bound species. The precipitate was then re-dispersed in distilled water, ensuring removal of unreacted luminol and metal salts. The purified Ce–Lum nanoparticles were stored at room temperature for further characterization and sensing experiments.

Standard Ce-metal aggregated luminol solution preparation

A standard Ce–metal aggregated luminol solution was prepared by accurately weighing 1.25 mg of purified Ce–Lum nanoparticles and transferring it into a 25 mL volumetric flask. The volume was adjusted using a buffer solution maintained at pH 9. The alkaline pH was selected because metal-aggregated luminol exhibits effective dissociation and activation only under basic conditions, which is essential for achieving a stable and reproducible fluorescence response. This standard solution was used for all subsequent morpholine sensing studies.

Characterization

Using a Perkin Elmer Lambda 35 spectrophotometer, UV-visible spectra were captured. A Jasco F8300 spectrofluorometer was used to acquire fluorescence spectra. A Thermo Scientific iS10 FT-IR spectrometer was used to measure the FT-IR spectra. and presented in absorption frequencies (cm^{-1}). A Rigaku Smart Lab diffractometer with CuKα radiation running at 40 kV and 30 mA was used to obtain X-ray diffraction (XRD) patterns. To ascertain elemental composition and oxidation states, an analysis using X-ray photoelectron spectroscopy (XPS) was employing a Kα Thermo Scientific apparatus that uses 180–200 W of Al Kα radiation. FE-SEM, or field emission scanning electron microscopy, was employed to use a Hitachi S-4800 device with an acceleration voltage of 10 kV to examine surface morphology.

Results and discussion

Structural characterization

The crystalline structure was examined by powder XRD analysis. and properties of the generated Ce-Lum compounds. XRD pattern of Ce-Lum shows a sharp peak [Fig. 1(a)] demonstrates crystalline nature and it confirms the presence of Ce metal along with oxygen in different oxidation states [23–25]. Using the Debye-Scherrer equation, the average crystalline size of the Ce-Lum nanoparticles was determined to be around 89 nm. where $D = K\lambda/\beta \cos\theta$, where D is the size of the crystal, the Scherrer constant, K, is 0.98, wavelength (1.54 nm) is represented by λ, and the full width at half maximum (FWHM) is represented by β [26].

FTIR (Fourier-transform infrared spectroscopy) spectrum showing [Fig. 1(b)] the transmittance of two samples: The FTIR spectra of both Luminol (blue curve) and the Ce-Lum composite (red curve) reveal several common absorption peaks, indicating the presence of similar functional groups. A broad peak around ~3350 cm^{-1} is observed in both samples, corresponding to N–H or O–H stretching vibrations, often associated with hydrogen bonding. Peaks near ~1650 cm^{-1} and ~1600 cm^{-1} can be attributed to C=O stretching (from amide or carbonyl groups) and C=C or N–H bending vibrations, respectively. Additionally, both spectra display bands from aromatic C=C stretching in the ~1450–1500 cm^{-1} range, as well as a clear peak at ~1380 cm^{-1} that most likely results from C–N stretching or CH_3 bending. Additional characteristic bands are found in the regions of ~1250–1300 cm^{-1} (C–N stretching of aryl amines), ~1100–1150 cm^{-1} (C–O or C–N stretching), ~1000–1050 cm^{-1} (out-of-plane bending), ~800–900 cm^{-1} (aromatic C–H bending), and ~600–700 cm^{-1}, corresponding to ring deformation or halogen-related vibrations. Notably, the Ce-Lum spectrum shows enhanced intensity and slight deviations in certain regions, particularly between 1100 and 900 cm^{-1}, suggesting possible molecular interactions or structural modifications compared to pure luminol. Additionally, shifts and broadening of peaks such as those around ~1650 cm^{-1} and ~3350 cm^{-1} point toward hydrogen bonding, conjugation effects, or complexation within the Ce-Lum compound, indicating successful formation of a modified or composite structure.

When Ce and luminol are mixed, they exhibit varying particle sizes, which amply demonstrates how luminol is incorporated with Ce by aggregation. Figure 1(c) displays the Ce-Lum aggregated compound's FESEM images, which display the aggregated fibers morphology. Figure 1(d) displays the Ce-Lum aggregated compound's EDAX result. This verifies that every element is present in the ratio predicted for the Ce-Lum combination. This kind of nano porous structures having additional advantages including high specific area, which effectively improves the performance in environmental sensing.

X-ray photoelectron spectroscopy (XPS) was used to analyze and determine the chemical states of the elements contained in the synthesized Ce-Lum. Figure 2 displays the

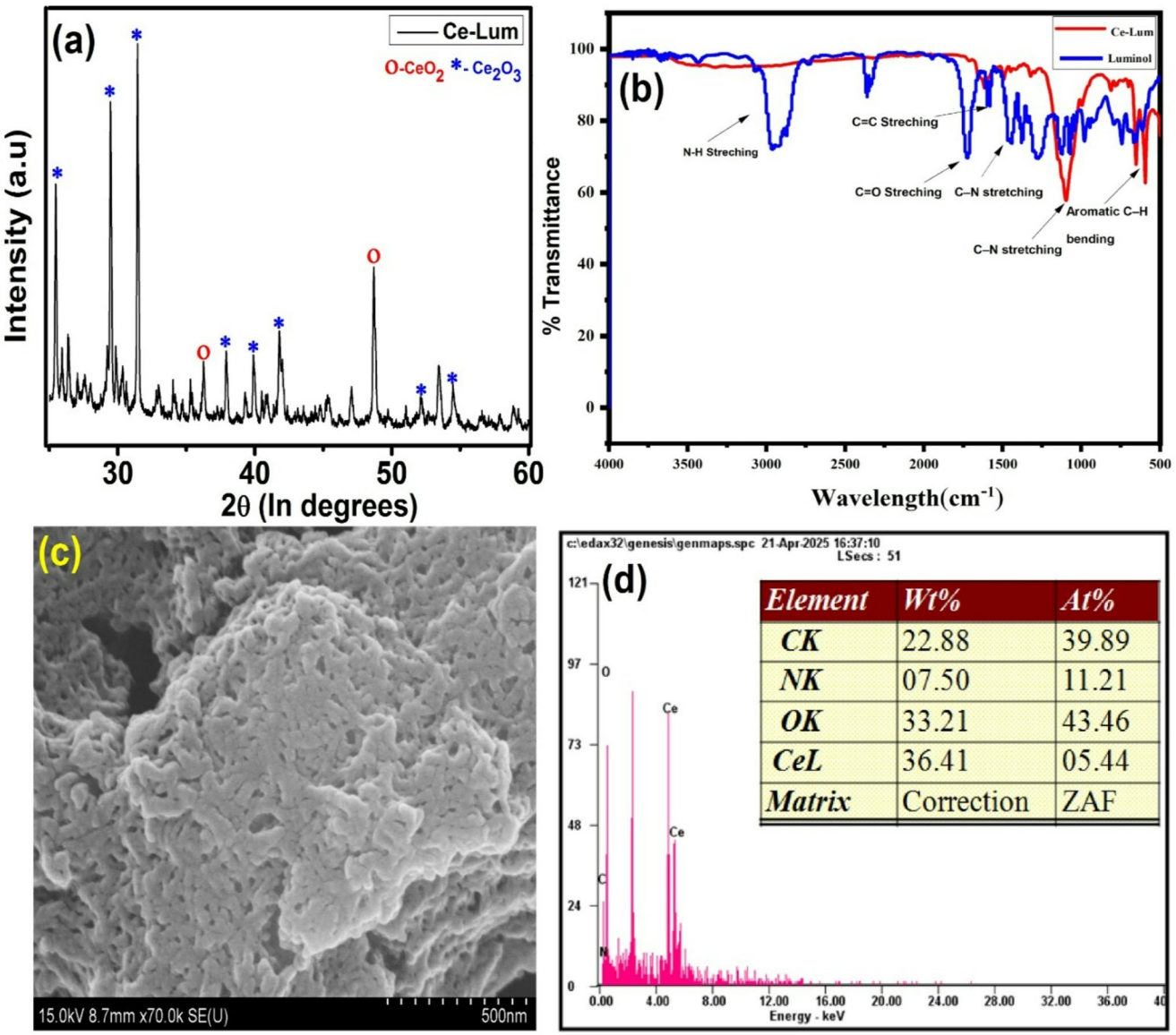

Fig. 1 (**a**) XRD images of Ce-Lum, (**b**) FT-IR image of Luminol and Ce-Lum, (**c**) SEM image of Ce-Lum, and (**d**) EDAX image of Ce-Lum

deconvoluted results. The survey spectrum [Fig. 2(a)], confirms the existence of several spin states for cerium, nitrogen, carbon, and oxygen. The Ce 3d spectrum at high resolution [Fig. 2(b)] shows, in accordance with earlier observations [27–29], a doublet for Ce3d5/2 and Ce3d3/2 at 885 eV and 904 eV, respectively, with a peak separation of 19 eV. Ce-O bonding is shown by a peak in the O1s spectrum [Fig. 2(c)] at 531.7 eV, which is in good agreement with the XRD finding. The XPS results confirm the Ce-Lum aggregation, in agreement with the XRD data. A signal at 399.3 eV in the high-resolution N1s spectra [Fig. 2(d)] indicates Ce-Lum aggregation. The Ce-Lum aggregation of the synthesized molecule is further confirmed by the C1s spectra [Fig. 2(e)], which show peaks at 287.4 and 284.6 eV attributed to C-N and C = C bonding, respectively [30].

UV-visible spectroscopic study

The well-known chemiluminescent reagent luminol, is valued for its robust chemiluminescent properties and diagnostic utilities [31, 32]. Luminol was dissolved in 0.01 M NaOH to prepare a basic solution. Using a standard catalyst to oxidize luminol in an alkaline environment results in the formation of two different bands of absorption at 200 and 350 nm. $\pi - \pi^*$ transitions are indicated by these bands. Notably, the Ce-Lum complex exhibits a redshift in its absorption peak compared to free luminol. The $\pi - \pi^*$ transitions are also responsible for the increased absorption bands at 270 and 370 nm that are present in the generated Ce-Lum complex. These findings suggest that the Ce-Lum complexation has a substantial effect on luminol's optical

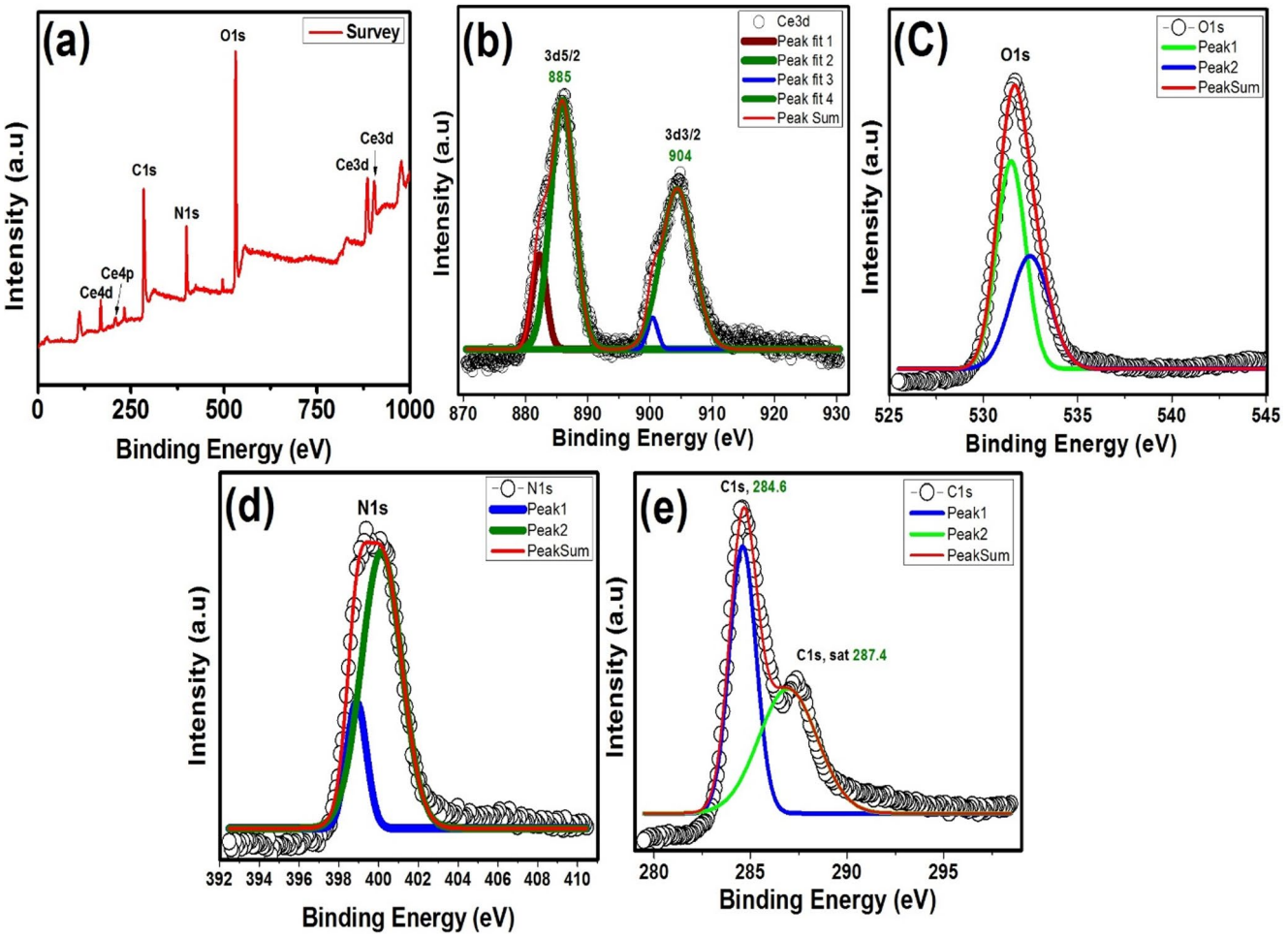

Fig. 2 XPS spectrum of Ce-Lum compound, (**a**) survey spectrum, high resolution spectrum of (**b**) Ce3d, (**c**) O1s (**d**) N1s and (**e**) C1s

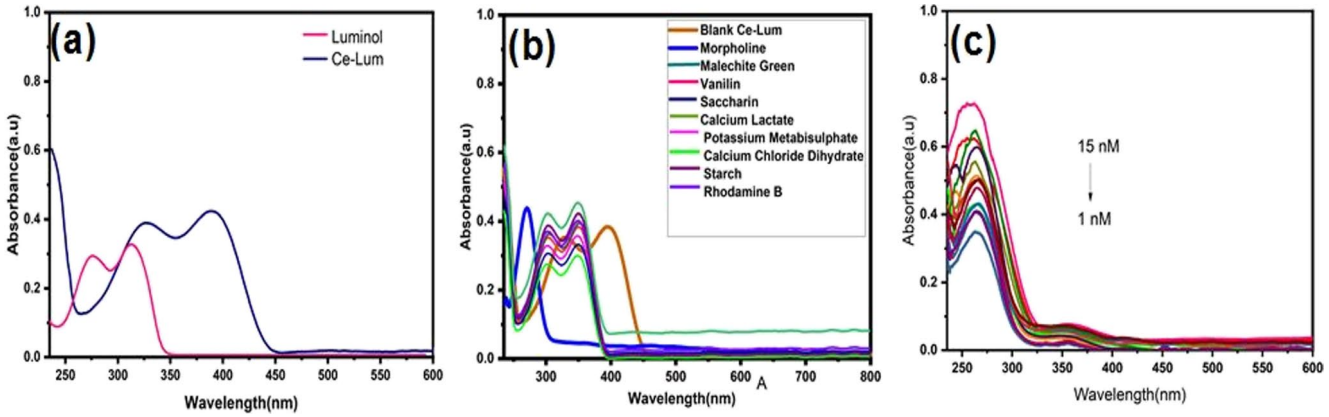

Fig. 3 (**a**) UV-Visible spectrum of luminol and aggregated Ce –Lum, (**b**) UV–Visible spectra of selectivity study using aggregated Ce-luminol with different analytes, (**c**) UV- visible spectra of Ce-Lum in the presence of increasing concentration of morpholine from 1 nM – 15 nM

characteristics. This enhancement is likely due to the complex's superior electronic conduction properties compared to conventional systems (Fig. 3a). These interactions don't seem to have a big impact on luminol's conjugated system, which mostly controls its UV-visible absorption properties, even though FT-IR spectra show alterations suggestive of chelation. Ce-Lum complex in the provided UV-visible absorption spectrum demonstrates a bathochromic shift (red shift) compared to free luminol, indicating an interaction between Ce ions and luminol. This shift suggests that

the coordination between cerium and luminol modifies the electronic environment, while retaining the characteristic electronic transitions of luminol. This shift could imply enhanced stability, changes in the molecular orbital energy levels, or chelation effects in the Ce-Lum complex, making it suitable for sensing applications.

The UV-visible spectrum displayed in the graph compares the absorbance of the Ce-Lum complex (Blank Ce-Lum) and different additives as an analyte in the 200–800 nm wavelength range [Fig. 3(a)]. Absorption spectrum for the Ce-Lum complex, without any additives, shows distinct peaks in the UV region, indicative of its electronic transitions. In order to investigate the selectivity of 10 µl of several additives, including morpholine, malachite green, vanillin, saccharin, calcium lactate, potassium metabisulfite, calcium chloride dihydrate, starch, and rhodamine B were put into 1.5 ml of Ce-Lum. Morpholine (Blue) Shows a noticeable alteration in absorbance around the UV region, potentially due to interactions affecting the Ce-Lum electronic environment. Blue fluorescence in the Ce-Lum solution, even after the addition of various additives, indicates that the electronic transitions responsible for spectra remain largely unaffected [Fig. 3(b)]. However, the exception observed with morpholine suggests a specific interaction between morpholine and the Ce-Lum that alters its properties. Its use for selective morpholine detection was confirmed by quantitative analysis and validation conducted under various morpholine concentrations. The effect of varying morpholine concentrations on the Ce-Lum's absorbance is demonstrated by the UV-visible absorption spectra. As the concentration increases (1 nM to 15 nM), there is a systematic increase in absorbance intensity, particularly in the UV region 250–400 nm [Fig. 3(c)].

This implies that the analyte and the Ce-Lum complex interact directly, changing the electronic environment of the complex. No significant shift in the wavelength of the absorption maxima is observed, indicating that the interaction primarily enhances the absorbance without altering the fundamental electronic transitions. The increase in absorbance with concentration suggests the potential for quantification of the analyte based on its interaction with Ce-Lum. The Ce-Lum complex could be utilized as a UV-visible sensor for detecting and quantifying analytes in nanomolar concentrations. The high sensitivity observed (starting at 1 nM) makes this system ideal for trace-level detection.

Ce-Lum fluorescence experiments in relation to different solvents

The incident light's path length through the medium is increased by Ce-Lum aggregates that form in the solution and serve as scattering centers. This dispersion enhances the way light interacts with Ce-Lum aggregates, increasing the total signal of absorption, rather than making an electrical connection directly. Figure 4(a) shows that the emission intensity of the Ce-Lum complex was 48 times higher than that of the parent luminol molecule, which fluorescence at a wavelength of 425 nm. In contrast to a parent Luminol, Resonant interactions between nearby molecules may be observed in aggregated Ce-Lum. which could increase the emission signal. The dipole interactions between the aggregate's closely spaced Ce-Lum molecules are what cause for these resonance effects, which may lead to new collective oscillation modes in response to light. The aggregate structure of Ce-Lum is very helpful for applications like detection systems that need a stronger signal. Nevertheless, the distinctive peak at 425 nm remains unchanged since these processes do not alter luminol's intrinsic electrical structure.

To examine selectivity in morpholine sensing, tests using fluorescence emission were carried out [33]. To the known taken quantity of Ce-Lum, a number of analytes were added, and their fluorescence emissions were tracked. These analytes included morpholine, malachite green, vanillin, saccharin, calcium lactate, potassium meta bisulphate, calcium chloride dihydrate, starch, and rhodamine B. At 425 nm, Ce–Lum exhibits a noticeable single emission band as shown in Fig. 4(a). When many analytes, including Malachite green, Vanillin, Saccharin, Calcium Lactate, Potassium Meta Bisulphate, Calcium Chloride Dihydrate, Starch, and Rhodamine B, are added to the Ce-Lum solution, the fluorescence emission wavelength at 479 nm can only be eliminated by morpholine [Fig. 4(c)]. Only morpholine has the ability to extinguish the fluorescence emission wavelength at 479 nm [Fig. 4(b)], and its fluorescence intensity is subdued.

Figure 4(d) illustrates the stability of the Ce-Lum NPs by monitoring the fluorescence intensity of the same batch of nanoparticle solution after different storage periods. The fluorescence spectra were recorded at regular time intervals under identical experimental conditions. As shown in the figure, no significant decrease in fluorescence intensity is observed over the studied storage duration, indicating that the optical properties of the Ce-Lum NPs remain largely unchanged. The minor variations in intensity fall within acceptable experimental error, confirming the good storage stability of the sensor. These results demonstrate that the Ce-Lum NPs possess adequate stability for practical sensing applications.

Should morpholine and the Ce-Lum aggregation combine to produce a stable combination, there might be fewer available excited-state molecules capable of fluorescence. Relaxing to the ground state is not necessary for this type of quenching; It occurs directly from the condition of agitation. In non-radiative energy transfer mechanisms, morpholine

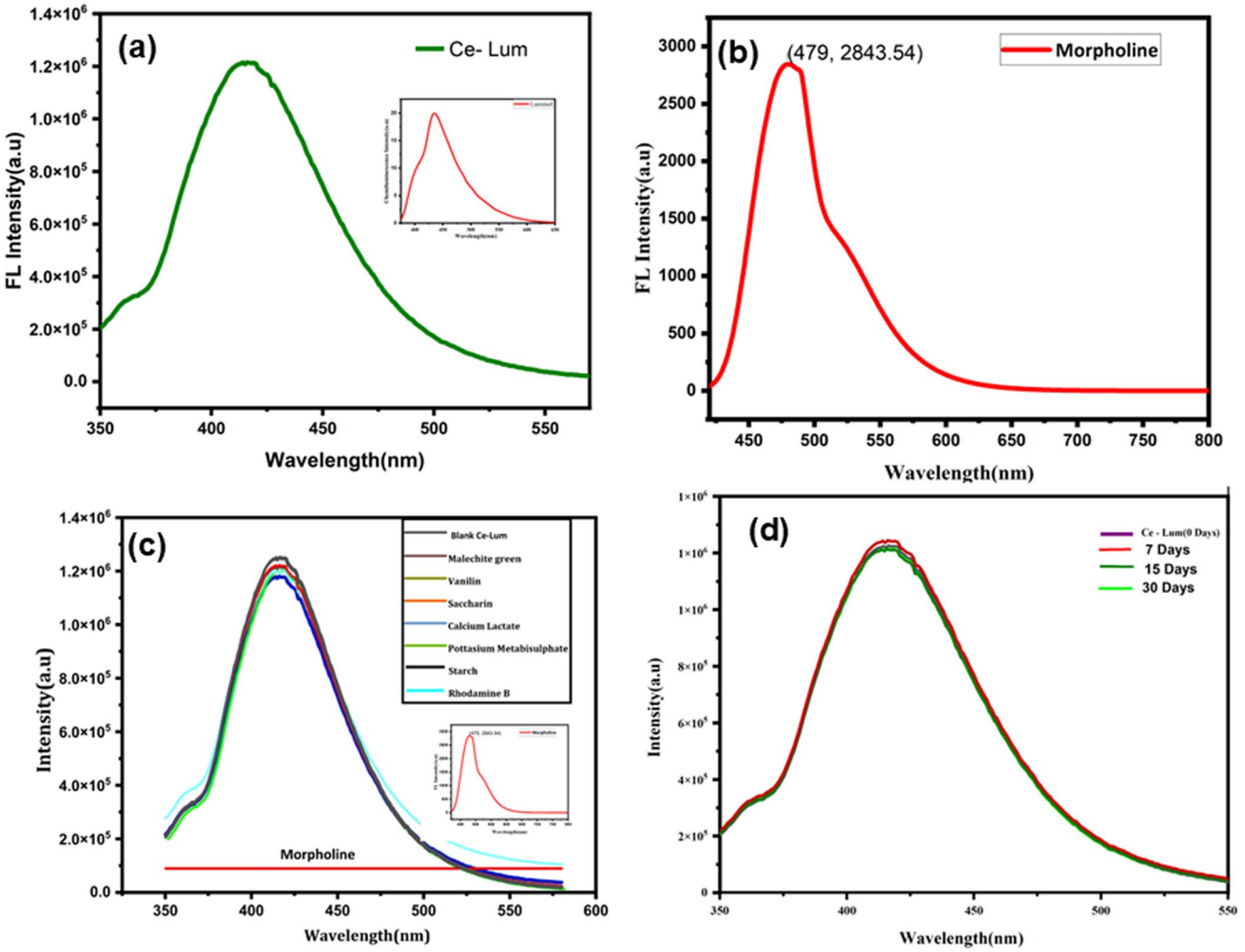

Fig. 4 (**a**) Fluorescence spectrum of Ce-Lum and luminol (inserted), (**b**) fluorescence-based sensing response of the Ce-Lum complex upon interaction with morpholine, (**c**) selectivity study of fluorescence spectra of Ce-Lum

may collide with the excited Ce-Lum species, deactivating the excited state before it can release light. The Ce-Lum's selective quenching effect makes it a viable option for morpholine detection because the amount of morpholine may be related to the degree of fluorescence quenching.

Morpholine may change the Ce-Lum complex's local environment, which would affect its fluorescence characteristics. Given that the degree of fluorescence quenching is associated with morpholine concentration, this selective quenching action raises the possibility that the Ce-Lum complex could be used as a probe for morpholine detection. To investigate this effect, the emission spectra of Ce-Lum were analysed at varying morpholine concentrations (1–10 nM). As depicted in Fig. 5(a), concentration-dependent decrease in fluorescence intensity was observed, whereas the emission wavelength remained constant. Morpholine does not substantially change the Ce-Lum complex; rather, the quenching is probably the consequence of a static or dynamic process that lowers the yield of fluorescence without altering the quantities of emission energy. This implies a strong contact without changing the structure of the excited state. The Ce-Lum complex may be a sensitive morpholine sensor as a result of this action, especially when exact concentration monitoring is required.

As illustrated in Fig. 5(b), The intensity of the fluorescence drastically dropped when Ce-Lum was used to titrate the morpholine. The response was linear, Having a 0.944 R^2 value [34]. By examining the intensity curve of fluorescence at 479 nm with morpholine concentration, the limit of detection was ascertained by applying Eq. (1).

$$Detection\ Limit\ =\ 3\sigma/k \tag{1}$$

where σ is the standard deviation of the blank measurement and k is the slope of the calibration curve [35]. The blank measurement's standard deviation (σ) was computed using recordings of around ten Ce-Lum (1.2×10^6 M) fluorescence spectra. The detection limit, which was calculated

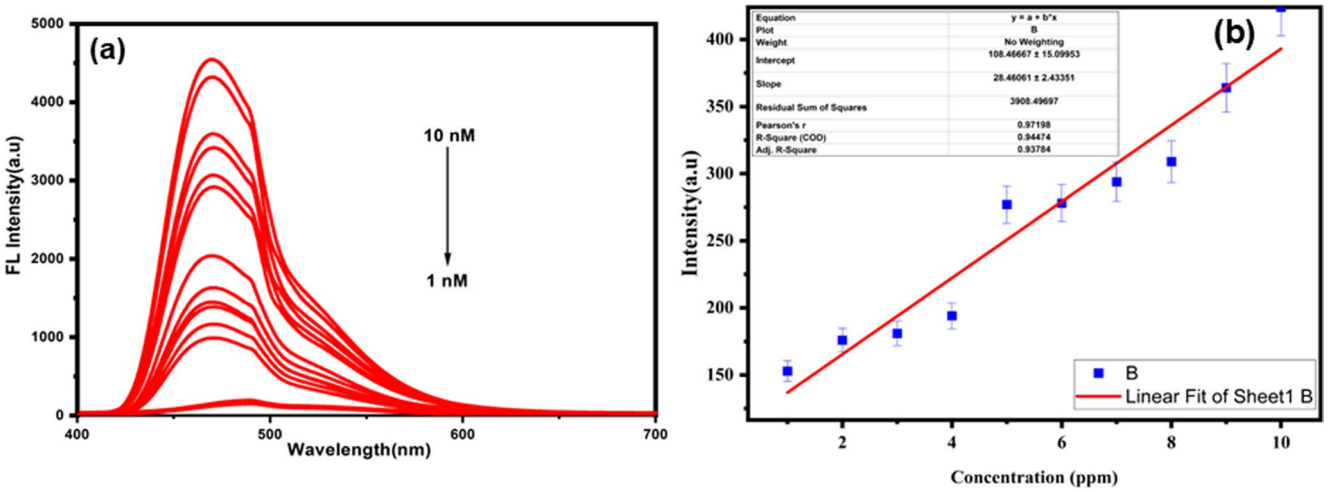

Fig. 5 (**a**) Emission spectra of Ce-Lum in the presence of increasing concentration of morpholine from 1 to 10 nM, (**b**) linearity plot of FL Intensity vs. morpholine concentration from 1 to 10 nM

using Eq. (1) above, was 0.08 ppb, indicating the Ce-Lum's high sensitivity to morpholine. The capacity to identify morpholine at such low levels may have important ramifications for environmental monitoring, clinical diagnostics, and safety assessments in industries that employ goods containing morpholine [36].

The qualitative comparison and the key differences between the proposed Ce-Lum based fluorescence sensor and conventional analytical techniques such as GC–MS and HPLC, as reported in the literature. Chromatographic methods are well known for their high sensitivity and accuracy; however, they typically require expensive instrumentation, complex sample preparation procedures, and trained personnel, resulting in longer analysis times and limited suitability for rapid or on-site detection. However, despite its widespread adoption and proven efficacy, GC–MS data analysis remains challenging due to the inherent complexity and large volume of data generated, as well as issues such as co-eluting peaks, noise, and baseline fluctuations. These factors complicate the extraction of meaningful chemical information and can compromise accurate quantification and structural elucidation of analytes. Moreover, when comparing multiple samples to identify discriminatory compounds, retention-time shifts between samples represent a significant analytical bottleneck. Although mass spectral matching is a powerful tool for peak alignment in targeted analyses, untargeted GC–MS studies frequently involve compounds with similar chemical structures that produce comparable mass spectra. This similarity can lead to inaccuracies in peak alignment, particularly for closely eluting species. Consequently, the reliability of qualitative and quantitative information obtained from GC–MS directly affects the accuracy of subsequent statistical analyses, biomarker discovery, pathway analysis, and data interpretation.

In contrast, the proposed fluorescence sensing approach offers a simpler and faster analytical strategy with lower operational complexity and cost. The short response time and minimal sample pretreatment make the sensor potentially suitable for routine and on-site applications. Although no direct experimental comparison with GC–MS or HPLC is performed in this study, the qualitative advantages highlighted are consistent with widely reported characteristics of fluorescence-based sensing systems, supporting the practical relevance of the developed sensor.

Possible reaction mechanism

By scavenging intermediates that are reactive or altering the route of the reaction, morpholine may function as a quenching agent and lessen luminol's chemiluminescence. Morpholine functions as a reducing agent that can efficiently stop the production of light by reacting with intermediates or reactive oxygen species (ROS) [37]. The Ce-Lum combination generates a monoanion when exposed to basic circumstances (OH^-). The molecule's structural modifications, which allow for further reactions, emphasize this intermediate. An extra intermediate is created when the monoanion combines with singlet oxygen ($^1O_2$). The route is altered when morpholine is added to the system because it reacts with $^1O_2$. In the absence of morpholine, the pathway proceeds with a low level of fluorescence intensity.

Morpholine contains a tertiary amine with a lone pair of electrons located at the nitrogen atom, corresponding to a relatively high-energy highest occupied molecular orbital (HOMO). The Ce-Lum material presents surface-exposed Ce^{3+}/Ce^{4+} centers with accessible empty or partially filled 4f/5d orbitals, which act as low-lying acceptor states upon photoexcitation. When morpholine approaches the Ce-Lum

surface, coordination occurs via donation of the nitrogen lone pair into these cerium-centered orbitals, resulting in the formation of a weak ground-state surface complex.

Upon excitation of Ce-Lum, this coordination interaction enables an energetically favourable non-radiative electron or energy transfer pathway governed by HOMO–LUMO alignment. Specifically, the excited-state electrons of Ce-Lum can be transferred to the LUMO of the coordinated morpholine molecule, or alternatively, the HOMO of morpholine can donate electrons to surface Ce^{4+} states, facilitating excited-state charge separation. In both scenarios, the radiative recombination pathway of Ce-Lum is effectively suppressed, leading to fluorescence quenching (Fig. 6).

Additionally, the formation of the coordination complex can introduce new interfacial energy levels that enhance internal conversion and vibrational relaxation processes, further increasing non-radiative decay. Such HOMO–LUMO–driven coordination-induced quenching mechanisms have been widely reported for amine-containing analytes interacting with metal-based luminophores and are often classified as static or surface-mediated quenching processes rather than ROS-dependent pathways. Therefore, the observed fluorescence quenching in the presence of morpholine can be reasonably attributed, at least in part, to coordination-induced electronic interactions arising from favourable energy-level alignment [38]. A decrease in intensity of fluorescence accompanied by a wavelength shift at 479 nm could occur if the excited luminol or Ce-Lum complex is briefly bound or interacts with the morpholine. In a sensing application, morpholine can reduce the luminol-based molecules or Ce-Lum's fluorescence by blocking catalysis, scavenging intermediates, or causing non-radiative decay. Since the signal drop caused by the quenching effect is proportional to the morpholine level, it may be used to assess morpholine concentration [39].

Real sample analysis: application to fruits peel extracts

Fresh fruits were collected from a local market, thoroughly washed with deionized water, and the peels were used for analysis. The fruit peels were soaked in 100 mL of deionized water in a 250 mL Pyrex beaker and heated at 45 °C for 30 min under gentle stirring. After soaking, the extract was allowed to cool naturally to room temperature and was then used for real-sample analysis.

The resultant solution was utilized for the selective analysis of spiking morpholine at concentrations ranging from 1 to 10 nM after it had cooled to room temperature. For the detection of morpholine, the Ce-Lum combination showed exceptional selectivity and anti-interference qualities. Even when different metal cations are present, (e.g., Cr^{3+}, Fe^{3+}, Mg^{2+}, Na^{+}, Ca^{2+}, Mn^{2+}, $Fe^{2+}$and Cu^{2+}), anions (e.g., NO_2^-, CO_3^{2-}, $S_2O_3^{2-}$, Cl^- and SO_4^{2-}), and organic compounds (e.g., cyclopentanone, cyclohexanone, glycine, aspartate, glucose, benzaldehyde, acetaldehyde, and acetylacetone) no significant fluorescence changes were observed (as shown in Fig. 7a). All interference and morpholine measurements were performed in triplicate under identical experimental conditions, and the error bars represent the standard deviation (± SD) of three independent measurements.

The inclusion of error bars improves the statistical reliability and clarity of the interference study and further confirms that morpholine produces a significantly distinct quenching response compared to other potential interferents.

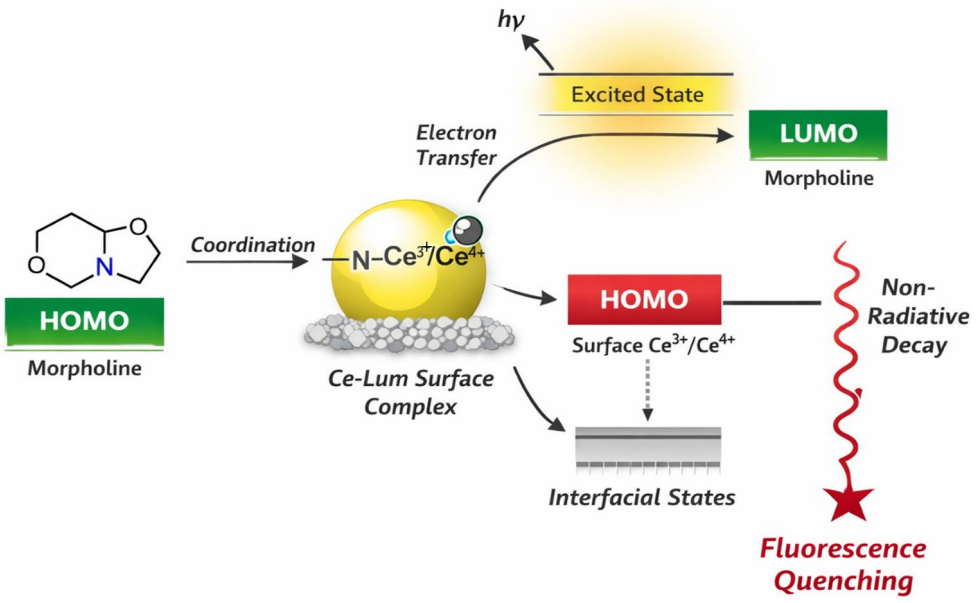

Fig. 6 (**a**) Anti-interference study, (**b**) fluorescence response of the probe in normal and spiked samples. Fluorescence intensity of the probe was measured in both normal (F0) and polluted (F) samples, with excitation and emission wavelengths of 350 nm and 425 nm, respectively

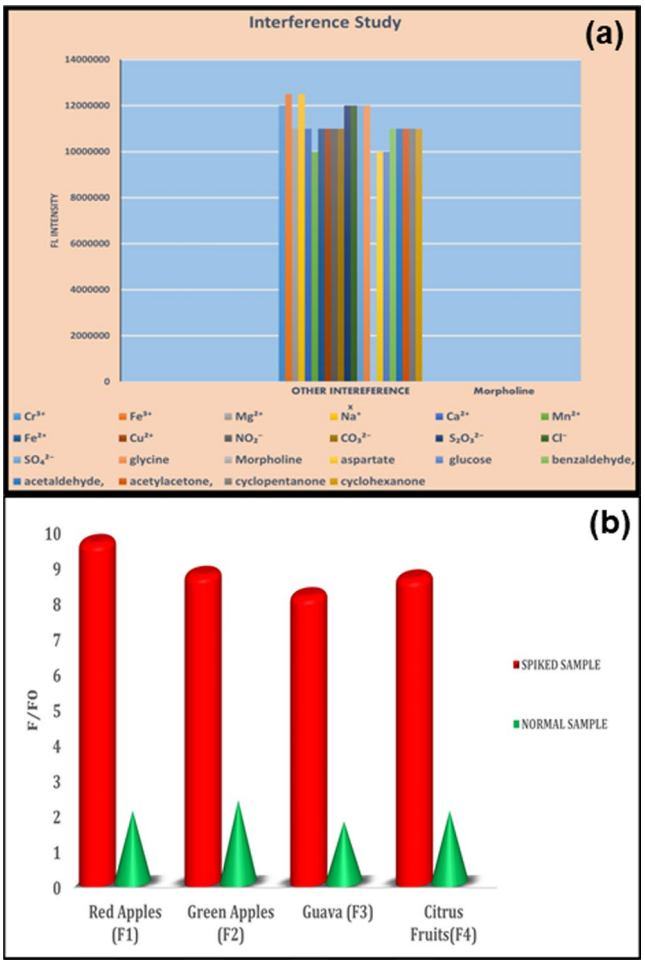

Fig. 7 (**a**) Anti-interference study of the fluorescent probe. Error bars represent the standard deviation ($n=3$). (**b**) Comparison of fluorescence response (F/F_0) for normal and morpholine-spiked fruit samples. Error bars represent the standard deviation of three independent measurements ($n=3$)

This excellent specificity suggests that the probe's capacity to detect morpholine is unaffected by these interferents. Even in complicated matrices with several chemicals, the Ce-Lum combination's strong selectivity and Anti-Interference ability make it a dependable instrument for morpholine identification.

Examining four distinct fruit samples fluorescence intensity (F1 to F4)-red apples, green apples, guavas, and citrus fruits-was carried out using two sample types: Green bars indicate boosted samples, whereas red bars indicate normal samples. The fruit samples are listed on the Y-axis, and the fluorescence intensity ratio (F/F_0), where the fluorescence intensity is denoted by F and the baseline intensity is F_0 is plotted on the X-axis. According to the data, all fruit varieties fluorescence intensity ratios are noticeably higher for spiked samples than for normal ones. This suggests the existence of an additional material or analyte, most likely morpholine or an analytical marker that intensifies fluorescence. The consistent fluorescence amplification in spiked samples across all fruit samples, as shown in Fig. 7b, demonstrates the method's effectiveness in identifying the analyte under spiking settings.

Validation study

Morpholine is commonly used in combination with fatty acids to create wax coatings that improve the appearance, shelf life, and resistance to moisture loss of fruits like apples. These coatings are particularly prevalent in commercially sold fruits to make them look shiny and fresh. Morpholine use in food coatings is banned in some regions, such as the European Union, due to potential health concerns. However, it is allowed in others, like the United States and Canada, within specific limits. Morpholine itself is relatively low in toxicity, but concerns arise because it can react with nitrites (found in the environment or some foods) to form carcinogenic nitrosamines. This has led to stricter regulation in some regions. Four fruit samples were used in a recovery experiment to test Ce-Lum's ability to identify morpholine in food samples. Each fruit's aqueous extract was utilized as the sample solution. The test system with the extracts was then supplemented with Ce-Lum. Two groupings of samples were created: blank specimens, devoid of morpholine and spiked samples with additional morpholine contaminants [40]. There were four types of fruits used to create a solution of fruit samples with values between 5 and 10 µg/ml (named F1, F2, F3, and F4) from various Chennai markets. A 2 ml cuvette was containing 1.8 milliliters of Ce-Lum (20 µM), followed by solutions of fruit samples with different quantities (5–10 µg/ml), in order to use our method to show how sensitive certain samples are. The corresponding FL was then noted. The linearity and accuracy of the method based on fluorescence data may be assessed by comparing the relevant concentration of the fruit sample solution to the fluorescence intensity at 479 nm. The regression equation was found after a linear calibration curve was created Additionally, the Relative Standard Deviation (RSD) was calculated to assess the measurement's accuracy. Three duplicates of every fruit sample were examined at the same dosage in order to verify the Ce-Lum FL procedure. For each fruit sample, 40 known concentrations were prepared, including 50%, 100%, 150%, and 200% impurity-spiked samples. The fluorescence responses were recorded, and the data was calculated using a spreadsheet. The recovery rates were then calculated using Eq. (2) [41].

$$Recovery\ (\%)\ =\ Observed\ value/True\ value \times 100 \qquad (2)$$

Table 1 Fruit sample morpholine detection

Samples	Recovery, %	Avg. Recovery	%RSD
50% of Sample 1	102.0	101.2	2.4
50% of Sample 2	98.5		
50% of Sample 3	103.2		
100% of Sample 1	101.5	102.7	1.6
100% of Sample 2	101.9		
100% of Sample 3	104.6		
150% of Sample 1	99.2	99.2	0.9
150% of Sample 2	98.3		
150% of Sample 3	100.1		
200% of Sample 1	98.3	99.0	0.7
200% of Sample 2	98.9		
200% of Sample 3	99.7		

The reproducibility and repeatability of the Ce-Lum FL sensor were evaluated by analysing three duplicates of each fruit sample at different spiked concentrations (50%, 100%, 150%, and 200%). The sensor demonstrated excellent repeatability, as reflected by low Relative Standard Deviation (RSD) values across all concentrations. Specifically, at 50% concentration, the average recovery was 101.2% with an RSD of 2.4%; at 100% concentration, the average recovery was 102.7% with an RSD of 1.6%; at 150% concentration, the average recovery was 99.2% with an RSD of 0.9%; and at 200% concentration, the average recovery was 99.0% with an RSD of 0.7%. These low RSD values indicate high reproducibility and consistent sensor performance across multiple measurements.

With a percentage RSD of 2.4 and an average of 101.2%, recovers at a 50% concentration range between 98.5% and 103.2%. With 102.7% on average and an RSD proportion of 1.6, the recoveries at 100% concentration are more densely clustered (101.5% to 104.6%). The range of recovery (98.3% to 100.1%) is more constrained at 150% concentration, resulting in an average of 99.2% and a percentage RSD of 0.9. With an average of 99.0% and a percentage RSD of 0.7, the recovery values (98.3% to 99.7%) are even more constant at 200% concentration (Table 1).

The recovery of the analyte was evaluated by spiking known amounts (50%, 100%, 150%, and 200% of the sample concentration) into three different samples. Each spiked sample was analyzed under the same experimental conditions, using excitation and emission wavelengths of 350 nm and 425 nm, respectively. The average recovery and percent relative standard deviation (%RSD) were calculated to assess the accuracy and precision of the method. The results show that the recovery ranged from 98.3% to 104.6% with % RSD values below 2.5%, indicating that the method is reliable and reproducible for the quantification of the analyte in various sample matrices.

Limitations and Future Research

While the Ce-Lum sensor demonstrates high sensitivity, selectivity, and rapid response for morpholine detection, potential limitations include interference from structurally similar or highly reactive substances present in complex sample matrices. Additionally, the current study focuses primarily on fresh fruits and vegetables, and its performance in other food types or environmental samples has yet to be systematically evaluated.

Future research could explore strategies to further improve selectivity, such as surface modification of the Ce-Lum nanoparticles or integration with complementary sensing techniques. Expanding the application to a wider range of food products, water, and environmental samples would help validate its versatility. Moreover, developing portable or on-site detection devices based on this sensor could enhance real-time monitoring capabilities in both industrial and environmental settings.

Conclusion

In summary, this work successfully uses the luminous qualities of luminol-capped Cerium nanoparticles to create a selective and highly sensitive for morpholine detection in fresh fruits and vegetables. The luminous response of the sensor is greatly improved by the incorporation of luminol, and the Cerium nanoparticles offer a reliable and effective detection platform. For precise morpholine monitoring, this sensor has proven to function exceptionally well, low detection limits, displaying quick reaction times, and extraordinary selectivity in complex sample matrices. The simple and efficient one-step synthesis of the Ce-Lum complex under ambient conditions, along with comprehensive characterization using techniques such as XRD, SEM, FTIR, and XPS, validates its potential as a reliable tool for morpholine detection. Beyond food products, the Ce-Lum sensor shows strong potential for broader applications, including food safety monitoring during storage and preservation, as well as environmental monitoring of pollutants. Its sensitivity, robustness, and reproducible recovery rates make it a practical tool for ensuring product quality, protecting consumer health, and supporting industrial and environmental safety efforts.

Its great sensitivity, resilience, and successful recovery rates are confirmed by experimental results, which make it a perfect choice for guaranteeing quality and food safety during preservation, particularly in samples obtained from nearby marketplaces. The results demonstrate the usefulness and effectiveness of this sensor, providing a useful way to preserve product quality and protect customer health.

Acknowledgements We gratefully acknowledge Entrepreneurship Development and Innovation Institute, entrusted Innovation Voucher Program (EDI - IVP) for their funding (Roc. No. II-01/44/2022/EDII/2022), Govt. of Tamil Nadu.

Author contributions S and R wrote the main manuscript text, D and S reviewed the manuscript.

Data availability No datasets were generated or analysed during the current study.

Declaration

Competing interests The authors declare no competing interests.

References

1. Kumari RK, Singh (2020) Morpholine as ubiquitous pharmacophore in medicinal chemistry: Deep insight into the structure-activity relationship (SAR). Bioorg Chem 96:103578. https://doi.org/10.1016/j.bioorg.2020.103578
2. Kerru N, Gummidi L, Maddila S, Gangu KK, Jonnalagadda SB (2020) A review on recent advances in nitrogen-containing molecules and their biological applications. Molecules 25:1909. https://doi.org/10.3390/molecules25081909
3. Shwetha KM, Praveen BM, Devendra BK (2024) A review on corrosion inhibitors: types, mechanisms, electrochemical analysis, corrosion rate and efficiency of corrosion inhibitors on mild steel in an acidic environment. Results Surf Interfaces 16:100258. https://doi.org/10.1016/j.rsurfi.2024.100258
4. Zhao X, Zhang J, Ma L, Wang W, Zhang M (2024) Study on the performance and mechanism of morpholine salt volatile corrosion inhibitors on carbon steel. Coatings 14(8):997. https://doi.org/10.3390/coatings14080997
5. Momtaz M, Bubli SY, Khan MS (2023) Mechanisms and health aspects of food adulteration: A comprehensive review. Foods 12:199. https://doi.org/10.3390/foods12010199
6. Yaashikaa PR, Kamalesh R, Kumar PS, Saravanan A, Vijayasri K, Rangasamy G (2023) Recent advances in edible coatings and their application in food packaging. Food Res Int 173:113366. https://doi.org/10.1016/j.foodres.2023.113366
7. Han C, Hu B, Huang C, Zhang W, Wu H, Liu C, Chen Q, Shen Y (2022) Determination of morpholine residue in fruit and fruit juices by gas chromatography–tandem mass spectrometry. LWT 161:113369. https://doi.org/10.1016/j.lwt.2022.113369
8. Cabrera LC, Piazza GD, Dujardin B, Marchese E, Pastor PM (2024) The 2022 European Union report on pesticide residues in food. Efsa J 22:1–91. https://doi.org/10.2903/j.efsa.2024.8753
9. Gavage M, Delahaut P, Gillard N (2021) Suitability of high-resolution mass spectrometry for routine analysis of small molecules in food, feed and water for safety and authenticity purposes: a review. Foods 10(3):601. https://doi.org/10.3390/foods10030601
10. Tienstra M, Hans GJ, Mol (2018) Application of gas chromatography coupled to quadrupole-orbitrap mass spectrometry for pesticide residue analysis in cereals and feed ingredients. J AOAC Int 101(2):342–351. https://doi.org/10.5740/jaoacint.17-0408
11. Belarbi S, Vivier M, Zaghouani W, Sloovere AD, Agasse-Peulon V, Cardinael P (2021) Comparison of new approach of GC-HRMS (Q-Orbitrap) to GC–MS/MS (triple-quadrupole) in analyzing the pesticide residues and contaminants in complex food matrices. Food Chem 359:129932. https://doi.org/10.1016/j.foodchem.2021.129932
12. Grund B, Marvin L, Rochat B (2016) Quantitative performance of a quadrupole-orbitrap-MS in targeted LC–MS determinations of small molecules. J Pharm Biomed Anal 124:48–56. https://doi.org/10.1016/j.jpba.2016.02.025
13. Varenina I, Bilandžić N (2022) Đurđica Božić Luburić, Božica Solomun Kolanović, and Ines Varga. High resolution mass spectrometry method for the determination of 13 antibiotic groups in bovine, swine, poultry and fish meat: An effective screening and confirmation analysis approach for routine laboratories. Food Control 133:108576. https://doi.org/10.1016/j.foodcont.2021.108576
14. Cao M, Zhang P, Feng Y, Zhang H, Zhu H, Lian K, Kang W (2018) Development of a method for rapid determination of morpholine in juices and drugs by gas chromatography-mass spectrometry. J Anal Methods Chem 1(2018):9670481. https://doi.org/10.1155/2018/9670481
15. Zhang X, Tang F, Zhang Y, Zhang P, Zhou W, Shu W, Xiao H (2024) A hemicyanine-based fluorescent probe for detection of pH and its applications in live cells imaging and food monitoring. Microchem J 200:110267. https://doi.org/10.1016/j.microc.2024.110267
16. Sharma A, Majdinasab M, Khan R, Li Z, Hayat A, Marty JL (2021) Nanomaterials in fluorescence-based biosensors: Defining key roles. Nano-Struct Nano-Objects 27:100774. https://doi.org/10.1016/j.nanoso.2021.100774
17. Tzara A, Xanthopoulos D, Kourounakis AP (2020) Morpholine as a scaffold in medicinal chemistry: an update on synthetic strategies. ChemMedChem 15:392–403. https://doi.org/10.1002/cmdc.201900682
18. Farzin MA, Abdoos H (2021) A critical review on quantum dots: From synthesis toward applications in electrochemical biosensors for determination of disease-related biomolecules. Talanta 224:121828. https://doi.org/10.1016/j.talanta.2020.121828
19. Zhao Q, Mei H, Li Y, Zhou P, Jing Q, Wang H, Wang X (2021) Sensitive detection of trace-level organophosphorus pesticides in fruit juices using a novel pH-responsive fluorescence probe based on 4-(morpholino methyl) phenyl) boronic acid. Microchem J 169:106541. https://doi.org/10.1016/j.microc.2021.106541
20. Zhao H, He Y, Lo Y, Song H, Lu J (2023) Fluorescent probes based on bioorthogonal reactions: Construction strategies and applications. TrAC Trends Anal Chem 169:117388. https://doi.org/10.1016/j.trac.2023.117388
21. Wu J, Lirong J, Verwilst P, An J, Zeng H, Zeng L, Niu G, Kim JS (2019) A colorimetric and fluorescent lighting-up sensor based on ICT coupled with PET for rapid, specific and sensitive detection of nitrite in food. Chem Commun 55:9947–9950. https://doi.org/10.1039/C9CC05048E
22. Peveler WJ, Yazdani M, Rotello VM (2016) Selectivity and specificity: Pros and cons in sensing. ACS Sens 1:1282–1285. https://doi.org/10.1021/acssensors.6b00564
23. Qin G, Cao D, Wan X, Wang X, Kong Y (2021) Polyvinylpyrrolidone-assisted synthesis of highly water-stable cadmium-based metal–organic framework nanosheets for the detection of metronidazole. RSC Adv 11:34842–34848. https://doi.org/10.1039/D1RA05349C
24. Wattanathana W, Suetrong N, Kongsamai P, Chansaenpak K, Chuanopparat N, Hanlumyuang Y, Kanjanaboos P, Wannapaiboon S (2021) Crystallographic and spectroscopic investigations on oxidative coordination in the heteroleptic mononuclear complex of cerium and benzoxazine dimer. Molecules 26(17):5410. https://doi.org/10.3390/molecules26175410
25. Qin G, Wang J, Li L, Yuan F, Zha Q, Bai W, Ni Y (2021) Highly water-stable Cd-MOF/Tb^{3+} ultrathin fluorescence nanosheets for ultrasensitive and selective detection of Cefixime. Talanta 221:121421. https://doi.org/10.1016/j.talanta.2020.121421

26. Vinila VS, Isac J (2022) Synthesis and structural studies of superconducting perovskite $GdBa_2Ca_3Cu_4O_{10.5+\delta}$ nanosystems. In: Thomas S, Kalarikkal N, Abraham AR (eds) Design, fabrication, and characterization of multifunctional nanomaterials. Elsevier, New York, pp 319–341. https://doi.org/10.1016/B978-0-12-820558-7.00022-4
27. Liu QQ, Yue KF, Weng XJ, Wang YY (2019) Luminescence sensing and supercapacitor performances of a new (3, 3)-connected Cd-MOF. CrystEngComm 21:6186–6195. https://doi.org/10.1039/C9CE01087D
28. Rahman MM, Alam MM, Alamry KA (2019) Sensitive and selective m-tolyl hydrazine chemical sensor development based on CdO nanomaterial decorated multi-walled carbon nanotubes. J Ind Eng Chem 77:309–316. https://doi.org/10.1016/j.jiec.2019.04.053
29. Solís RR, Gómez-Avilés A, Belver C, Rodriguez JJ, Bedia J (2021) Microwave-assisted synthesis of NH_2-MIL-125 (Ti) for the solar photocatalytic degradation of aqueous emerging pollutants in batch and continuous tests. J Environ Chem Eng 9:106230. https://doi.org/10.1016/j.jece.2021.106230
30. Cattaneo S, Naslhajian H, Somodi F, Evangelisti C, Villa A, Prati L (2018) Ruthenium on carbonaceous materials for the selective hydrogenation of HMF. Molecules 23(8):2007. https://doi.org/10.3390/molecules23082007
31. Alsharabasy AM (2025) Re-engineering Luminol: New Frontiers in Chemiluminescent Chemistry. Mol Syst Des Eng. https://doi.org/10.1039/D5ME00065C
32. Li H, Wang J, Du J (2021) A novel luminol chemiluminescence system induced by black phosphorus quantum dots for cobalt (II) detection. Talanta 223:121712. https://doi.org/10.1016/j.talanta.2020.121712
33. Nag S, Das D, Tudu B, Roy RB (2021) Multivariate analysis of formalin using UV-Vis spectroscopy. In: (2021) IEEE Second international conference on control, measurement and instrumentation (CMI). IEEE, pp 133–137. https://doi.org/10.1109/CMI50323.2021.9362970
34. Chibac-Scutaru A, Laura, Roman G (2024) Fluorescence sensing of metal ions in solution using a morpholine-containing phenolic Mannich base of 1′-hydroxy-2′-acetonaphthone. RSC Adv 14(52):38590–38604. https://doi.org/10.1039/D4RA07200F
35. Mei Q, Shi Y, Hua Q, Tong B (2015) Phosphorescent chemosensor for Hg^{2+} based on an iridium(iii) complex coordinated with 4-phenylquinazoline and carbazole dithiocarbamate. RSC Adv 5:74924–74931. https://doi.org/10.1039/C5RA09609J
36. Kourounakis AP, Xanthopoulos D, Tzara A (2020) Morpholine as a privileged structure: A review on the medicinal chemistry and pharmacological activity of morpholine containing bioactive molecules. Med Res Rev 40:709–752. https://doi.org/10.1002/med.21634
37. Su Y, Song H, Lv Y (2019) Recent advances in chemiluminescence for reactive oxygen species sensing and imaging analysis. Microchem J 146:83–97. https://doi.org/10.1016/j.microc.2018.12.056
38. Khan P, Idrees D, Moxley MA, Corbett JA, Ahmad F, von Ossowski G, Jameel NM et al (2014) Luminol-Based Chemiluminescent Signals: Clinical and Non-clinical Application and Future Uses. Appl Biochem Biotechnol 173(2):333–355. https://doi.org/10.1007/s12010-014-0850-1
39. Khan P, Idrees D, Moxley MA, Corbett JA, Ahmad F, Figura Gv, Sly WS, Waheed A, Hassan MI (2014) Luminol-based chemiluminescent signals: Clinical and non-clinical application and future uses. Appl Biochem Biotechnol 173:333–355. https://doi.org/10.1007/s12010-014-0850-1
40. Fappiano L, Carriera F, Iannone A, Notardonato I, Avino P (2022) A review on recent sensing methods for determining formaldehyde in agri-food chain: A comparison with the conventional analytical approaches. Foods 11:1351. https://doi.org/10.3390/foods11091351
41. Arshad B, Iqbal T, Akram S, Mushtaq M (2017) An expedient reverse-phase high-performance chromatography (RP-HPLC) based method for high-throughput analysis of deferoxamine and ferrioxamine in urine. Biomed Chromatogr 31:e3805. https://doi.org/10.1002/bmc.3805